Wave-current-turbulence interaction near the sea surface

Mostafa Bakhoday Paskyabi, Ilker Fer, Alastair D. Jenkins

Geophysical Institute
University of Bergen, Norway

Mostafa.Bakhoday@gfi.uib.no

Available Platforms (NORCOWE)

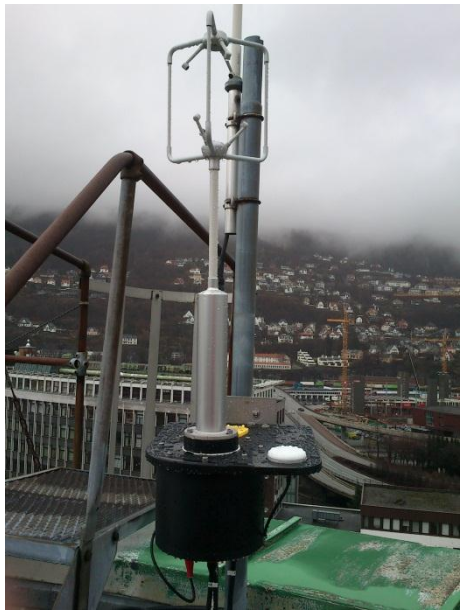

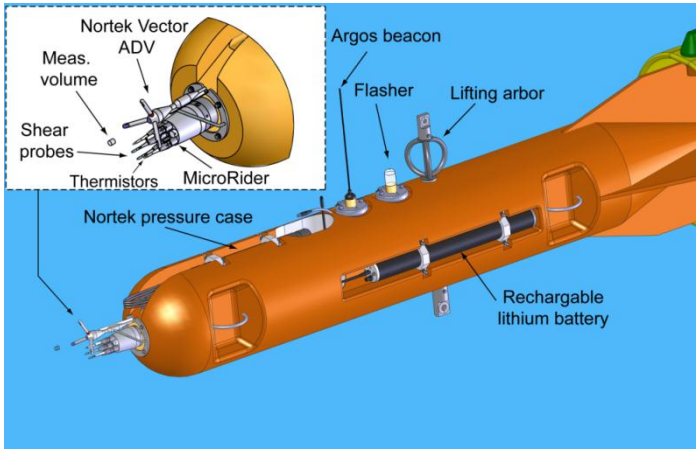

RPAS SUMO

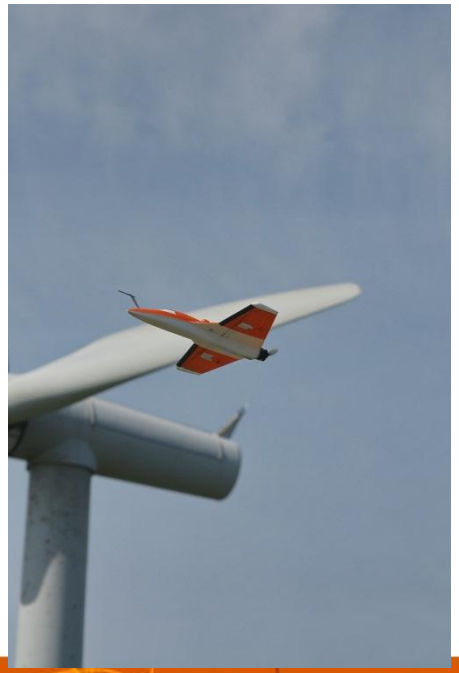

scanning wind lidar
Leosphere
WindCube 100S
(Dec. 2011)

Outline

1. Scientific background
2. Observations
3. Numerica modelling and parameterizations
4. Results: model-observation comparisons.
5. Conclusions

Background

- Upper ocean and large scale climate models

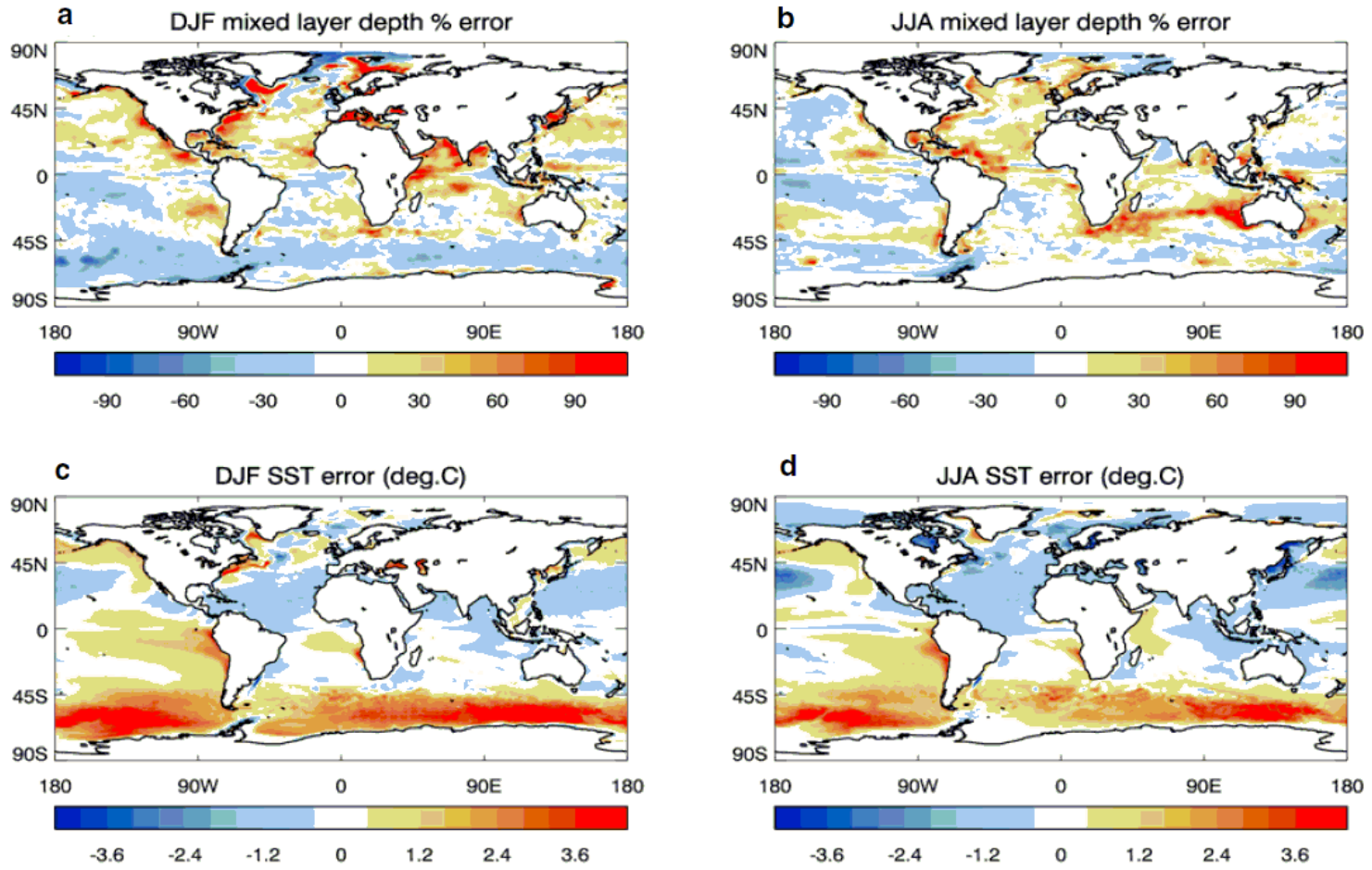

From Belcher et. al 2012

Background: upper ocean structure

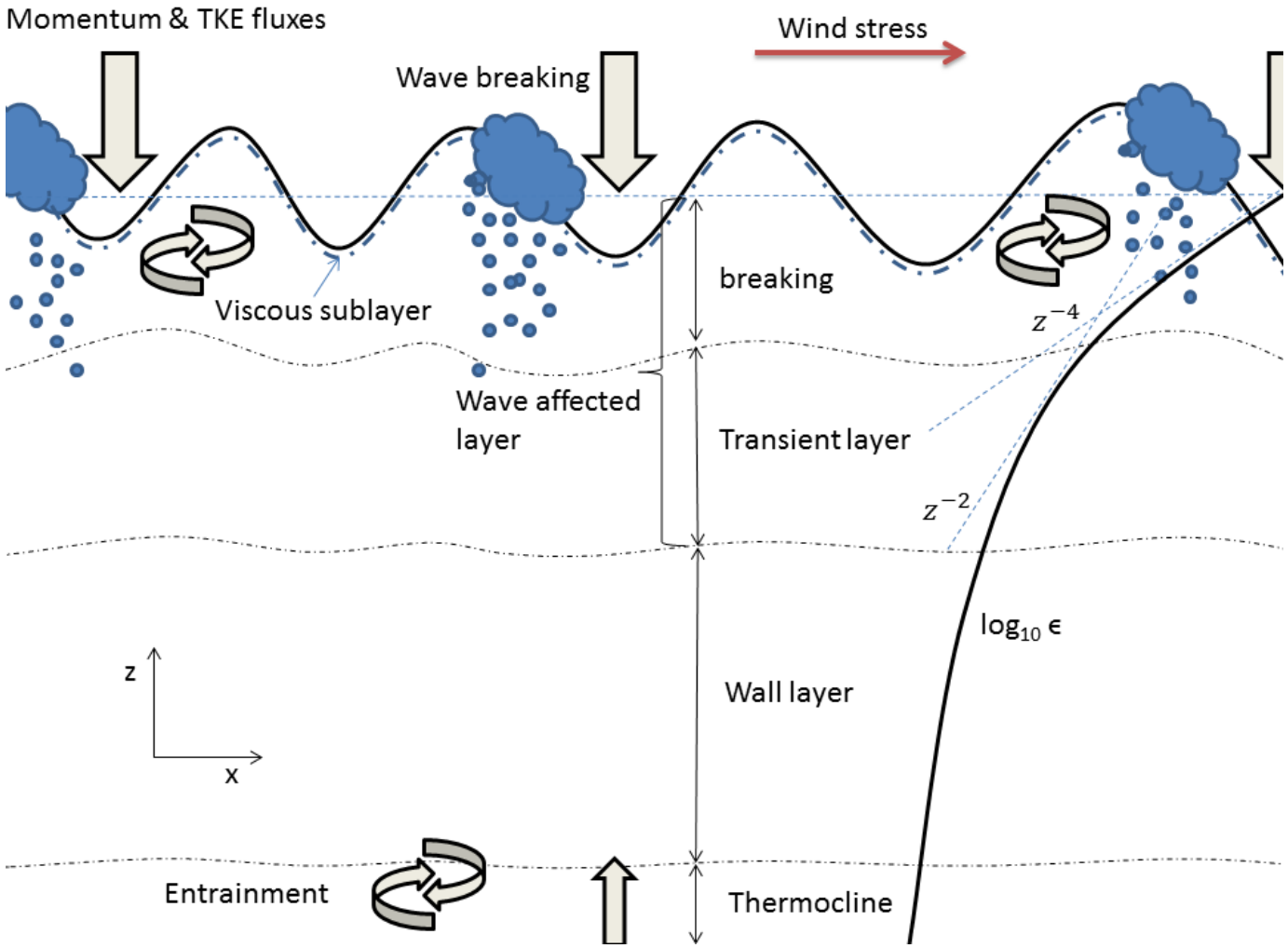

Wave induced forcing

$$\overline{u}_S \approx \omega k a^2 e^{2kz} = \frac{4\pi^2 a^2}{\lambda T} e^{4\pi z/\lambda}.$$

$$\tau = \tau_v + \tau_t + \tau_w.$$

$$\tau_w^x = p_0 \overline{\frac{\partial \zeta}{\partial x}}; \quad \tau_w^y = p_0 \overline{\frac{\partial \zeta}{\partial y}}, \qquad \boldsymbol{\tau}_w(f,\Theta) = \frac{S_{in}(f,\Theta)}{c_{ph}(f,\Theta)},$$

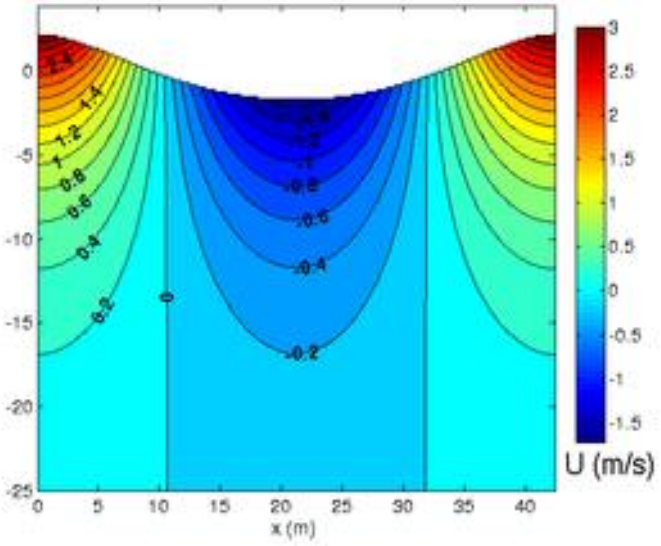

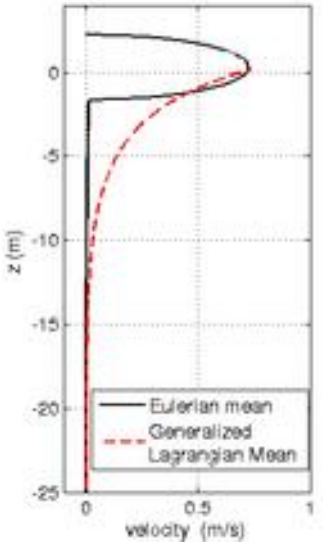

$$\mathbf{F}_{CSF} = -f_{cor} \times \mathbf{u}_s.$$

$$\frac{\partial E}{\partial t} + \frac{\partial}{\partial x}(Ec_g) = S_{in} + S_{ds} + S_{nl},$$

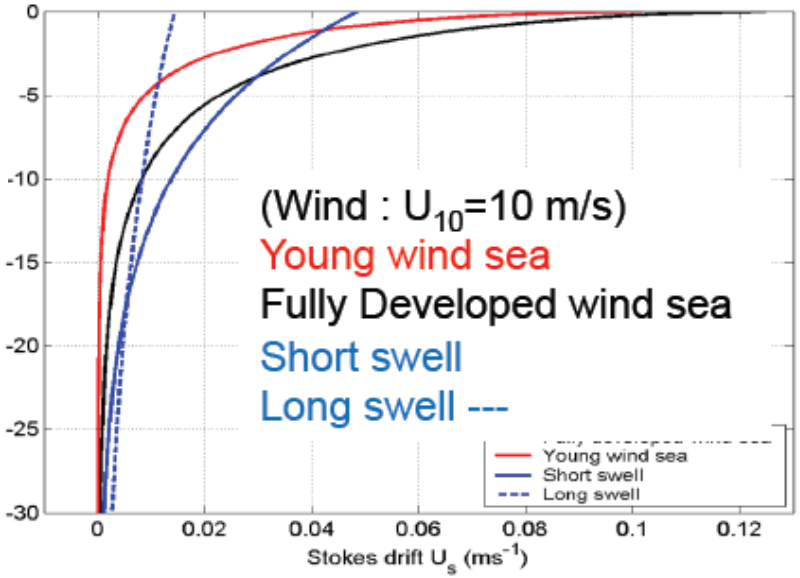

From Bakhoday-Paskyabi et al. 2012 (CSR)

From Rascle et. al 2006

Background: wave-wind-cuurrent-turbulence

$$T' \ll \tilde{T} \ll \bar{T}; \text{ and } X = X' + \tilde{X} + \overline{X},$$

- **Wave-wind interaction.**

$$\mathbf{u} = \bar{\mathbf{u}} + \tilde{\mathbf{u}} + \mathbf{u}', \text{ and } p = \bar{p} + \tilde{p} + p'$$

$$\frac{D\bar{u}_i}{Dt} = -\frac{1}{\rho_a}\frac{\partial \bar{p}}{\partial x_i} - \delta_{i3}g + \nu\frac{\partial \bar{u}_i}{\partial x_i} - \frac{\partial}{\partial x_j}(\overline{u'_j u'_i} + \overline{\tilde{u}_j \tilde{u}_i}),$$

$$\frac{1}{2}\frac{\partial \tilde{u}_i^2}{\partial t} = -\overline{\tilde{u}\tilde{w}}\frac{\partial \bar{u}}{\partial z} + \overline{< u'_i u'_j >}\frac{\partial \tilde{u}_i}{\partial x_j} - \frac{\partial}{\partial z}\left[\overline{\tilde{w}\left(\frac{1}{2}\tilde{u}_i^2 + \frac{\tilde{p}}{\rho}\right)} + \overline{< w' u'_i >}\,\tilde{u}_i\right],$$

$$\frac{1}{2}\frac{\partial u'^2_i}{\partial t} = -\overline{u'w'}\frac{\partial \bar{u}}{\partial z} - \overline{< u'_i u'_j >}\frac{\partial \tilde{u}_i}{\partial x_j} - \frac{\partial}{\partial z}\left[\overline{w'\left(\frac{1}{2}u'^2_i + \frac{p'}{\rho}\right)} + \overline{\left\langle\frac{1}{2}u'^2_i\right\rangle\tilde{w}}\right] - \varepsilon,$$

$$\frac{\partial e}{\partial t} = -\overline{u'w'}\frac{\partial \bar{u}}{\partial z}\overbrace{-\overline{\tilde{u}\tilde{w}}\frac{\partial \bar{u}}{\partial z}}^{1} + \frac{\partial}{\partial z}\left[\frac{1}{\rho}\overline{w'p'} + \overline{e'w'}\right]\overbrace{-\frac{1}{\rho}\frac{\partial \overline{\tilde{w}\tilde{p}}}{\partial z}}^{2} - \varepsilon = 0,$$

Background: wave-wind-cuurrent-turbulence

- **Wave-current interaction:**
  1. Vortex force effect.
  2. Radiation stress.
  3. Hybrid approach.

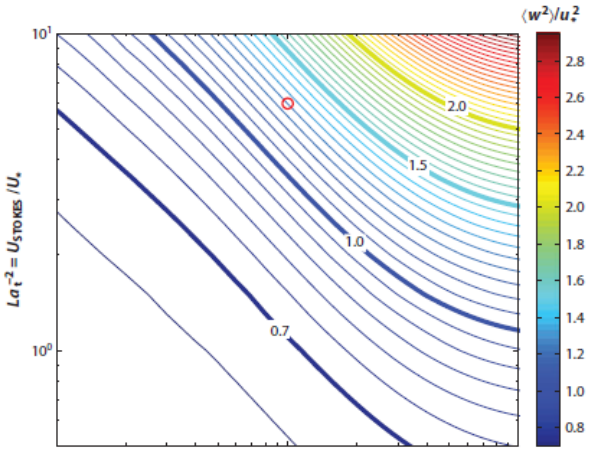

as

$$(\mathbf{q}.\nabla)\mathbf{q} = \frac{1}{2}\nabla(\mathbf{q}\cdot\mathbf{q}) - \mathbf{q}\times\boldsymbol{\omega},$$

where $\boldsymbol{\omega} = \nabla \times \mathbf{q}$ is the vorticity and $\mathbf{q} = (\mathbf{u}, w)$ is the Eulerian three–dimensional velocity. In the radiation stress representation, the advection term is expressed by

$$(\mathbf{q}.\nabla)\mathbf{q} = \nabla\cdot(\mathbf{q}\mathbf{q}) + \mathbf{q}(\nabla\cdot\mathbf{q}).$$

From D'asaro et. al 2013

Background: wave-wind-cuurrent-turbulence

- **Wave-current interaction:**
  1. Vortex force effect.

$$\frac{\partial \boldsymbol{\omega}_0}{\partial t_s} = \nabla \times (\mathbf{u}^s \times \boldsymbol{\omega}_0) + \nabla \times (\mathbf{v}_0 \times \boldsymbol{\omega}_0) + \nabla \times (\mathbf{v}_0 \times 2\boldsymbol{\Omega}) + \mathrm{La}\nabla^2 \boldsymbol{\omega}_0 + \cdots, \quad (2.13)$$

$$\mathbf{u}^s = \left\langle \int^{t_w} \widetilde{\mathbf{q}}(\cdot, s) ds \cdot \nabla \widetilde{\mathbf{q}} \right\rangle,$$

$$\frac{\partial \mathbf{q}}{\partial t} + \mathbf{q} \cdot \nabla \mathbf{q} = \mathbf{u}^s \times (\nabla \times \mathbf{q} + 2\boldsymbol{\Omega}) - \nabla \Pi + \mathrm{La}\nabla^2 \mathbf{q} + \cdots,$$

modified pressure (Bernoulli head) is expressed as

$$\Pi = p + \frac{1}{2}(\mathbf{q} + \mathbf{u}^s)^2.$$

Background: wave-wind-cuurrent-turbulence

- **Wave-current interaction:**
  1. Radiation stress.

Upon vertically integrating Eq. (2.1) from bottom ($z=-H$) to the surface ζ, using boundary conditions (Eqs. 2.4 and 2.5), and splitting the flow into the mean and wave components ($u_i=\bar{u}_i+\tilde{u}_i$, $p=\bar{p}+\tilde{p}$, and $\zeta=\overline{\zeta}+\widetilde{\zeta}$), the time average equations are obtained as:

$$\begin{aligned}\frac{\partial \overline{T}_i}{\partial t}+\frac{\partial \widetilde{T}_i}{\partial t} &= -\frac{\partial}{\partial x_j}\left(\int_{-H}^{\bar{\zeta}}\bar{u}_i\bar{u}_j dz+\int_{-H}^{\bar{\zeta}}\bar{p}\delta_{ij}dz\right)-\frac{\partial S_{ij}}{\partial x_j}\\ &- f_{cor}(\hat{z}\times\overline{T})_i-f_{cor}(\hat{z}\times\widetilde{T})_i+\tilde{p}(z=-H)\frac{\partial H}{\partial x_i}\\ &+ [\bar{p}(z=\bar{\zeta})-\tilde{p}(z=\bar{\zeta})]\frac{\partial\bar{\zeta}}{\partial x_i}+\cdots, \qquad (2.16)\end{aligned}$$

where

$$\begin{aligned}\overline{T}_i &= \int_{-H}^{\bar{\zeta}}u_i dz;\ \text{and}\ \widetilde{T}_i=\int_{\bar{\zeta}}^{\zeta}u_i dz,\\ S_{ij} &= \overline{\int_{-H}^{\zeta}(\tilde{u}_i\tilde{u}_j+\tilde{p}\delta_{ij})dz}-\overline{\int_{\bar{\zeta}}^{\zeta}(u_iu_j+P\delta_{ij})dz}. \qquad (2.17)\end{aligned}$$

Background: wave-wind-cuurrent-turbulence

- **Wave-wind interaction.**
  1. Hybrid approach.

$$z = z(x, y, s, t). \tag{2.18}$$

Now, any quantity can be expressed in the g–system using Eq. (2.18) and the chain rule. For example. the horizontal equation of motion (Eq. 2.1) can be transferred to the g–system by

$$\frac{\mathrm{D}\mathbf{u}}{\mathrm{D}t} + f_{cor}\hat{z} \times \mathbf{u} = -\frac{1}{\rho}\nabla^g P + \frac{1}{\rho}\left(\frac{\partial s}{\partial z}\right)(\nabla^g z)\frac{\partial P}{\partial s} + F, \tag{2.19}$$

Background: wave-turbulence interaction some aspects

1. near the sea surface, most of turbulent energy is concentrated in frequencies lower than the wave–affected frequency band;
2. there exists an inertial subrange with a slope of -5/3 for the turbulent spectra similar to those observed in the vicinity of a solid boundary;
3. wave orbital velocities, together with mean current advect turbulent eddies past a fixed point;
4. surface gravity waves dissipate energy locally through the wave breaking into the water column (with depths proportional to the scale of wave height) resulting in a substantial enhancement of TKE and its dissipation near the sea surface;
5. surface waves are not perfectly irrotational, i.e., the horizontal and vertical velocities are not in quadrature and there exist the wave–induced downward Reynolds stresses;
6. wave energy can be transferred to the turbulent field associated with attenuation of surface waves and non–breaking wave effects; and
7. wave–induced transport of TKE can be another responsible mechanism for the wave–turbulence interaction.

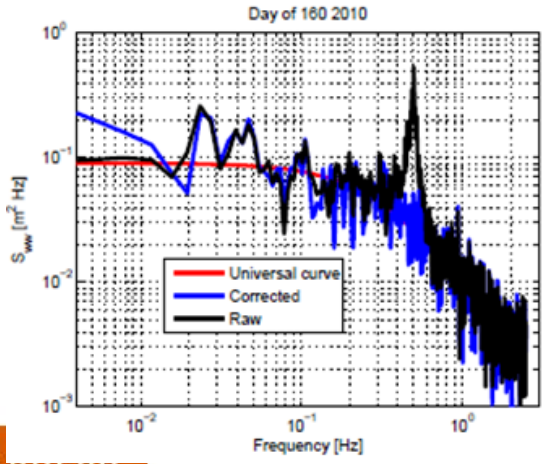

Observation of dissipation rates of TKE

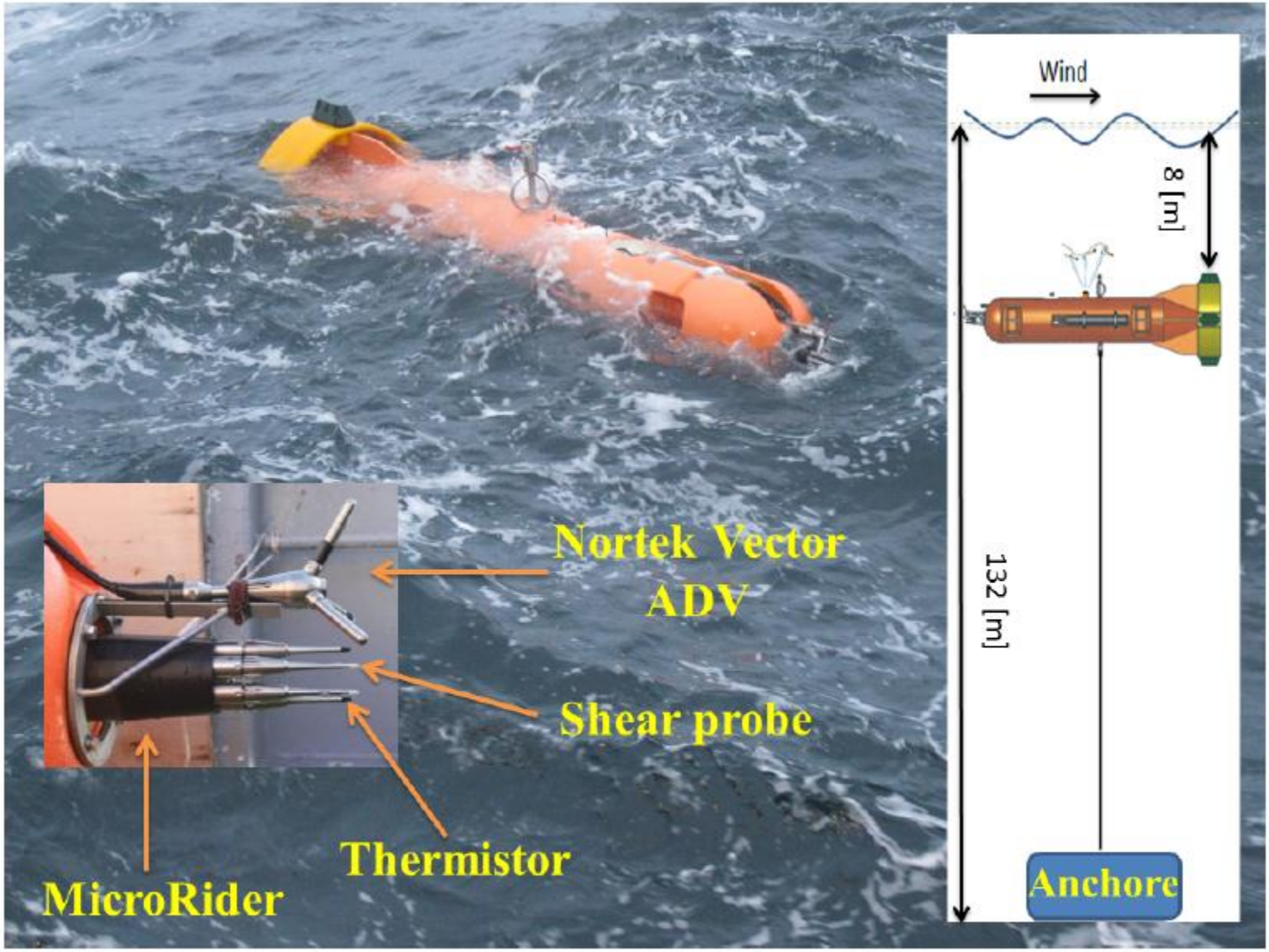

Fig. 1. Picture of MATS during the deployment together with a close up of the sensors (inset). The inset on the right shows the MATS mooring in the water column (not to scale).

Sample Turbulent Fluxes

Heat flux, $F_H = \rho_0 C_P \overline{w'T'}$

Salt flux, $F_S = \rho_0 \overline{w'S'}$

Buoyancy flux, $B = -(g/\rho_0)\overline{w'\rho'}$

Reynolds stress, $\tau = -\rho_0 \overline{w'u'}$

Eddy Correlation | **Shear (du/dz) variance** | **Scalar gradient (dT/dz or dC/dz) variance**

MAST / MOORED | **LOOSELY-TETHERED PROFILERS**

$\overline{w'T'}; \overline{w'C'}; \overline{w'u'}$

Suitable

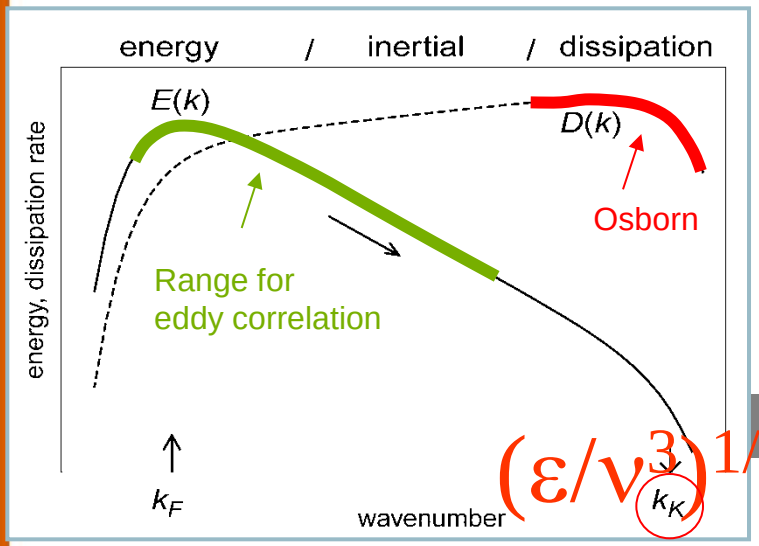

$$\varepsilon = \frac{15}{2}\nu\overline{\left(\frac{\partial u'}{\partial z}\right)^2}$$

$$K_\rho = \Gamma\frac{\varepsilon}{N^2}$$

$$\overline{w'\rho'} = -K_\rho\frac{\partial\overline{\rho}}{\partial z}$$

$$B = -K_\rho N^2$$

OSBORN MODEL

$$\chi = 6k_T\overline{\left(\partial T'/\partial z\right)^2}$$

$$-2\,\overline{w'T'}\,\frac{\partial\overline{T}}{\partial z} = \chi$$

$$K_T = 3k_T\frac{\overline{\left(\partial T'/\partial z\right)^2}}{\left(\partial\overline{T}/\partial z\right)^2}$$

$$F_H = -\rho_0 C_P K_T\frac{\partial\overline{T}}{\partial z}$$

OSBORN-COX MODEL

Site:
Havsul-1

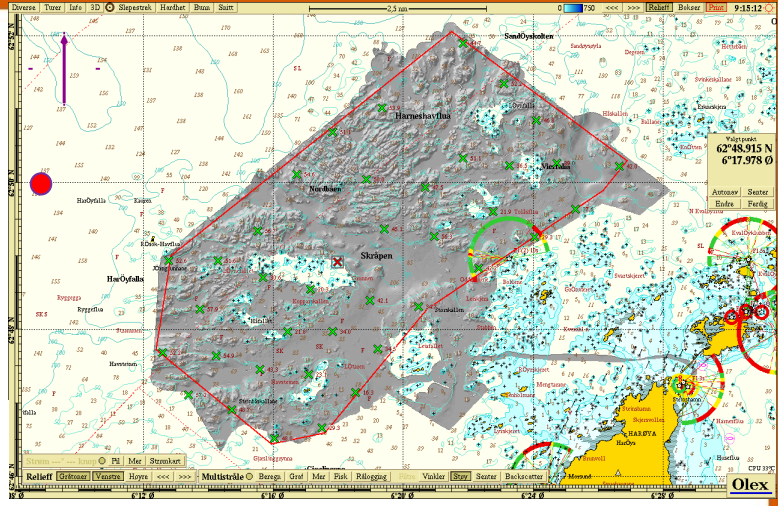

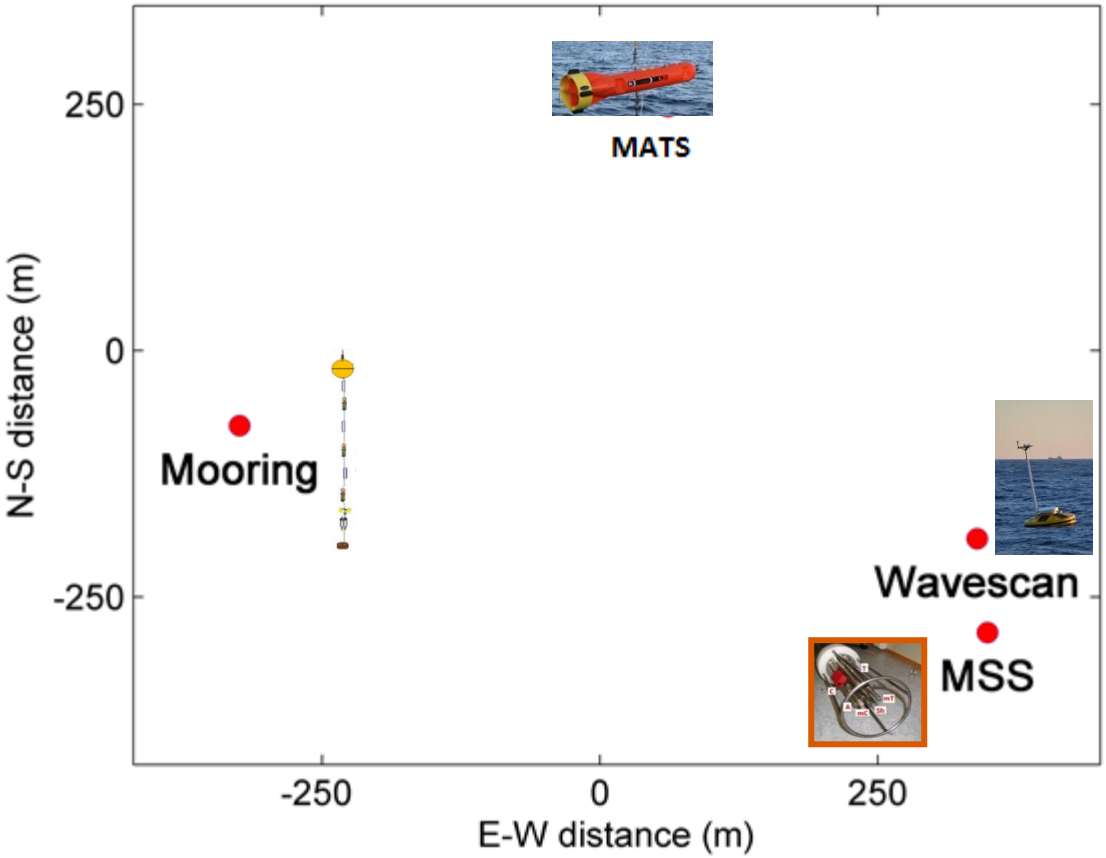

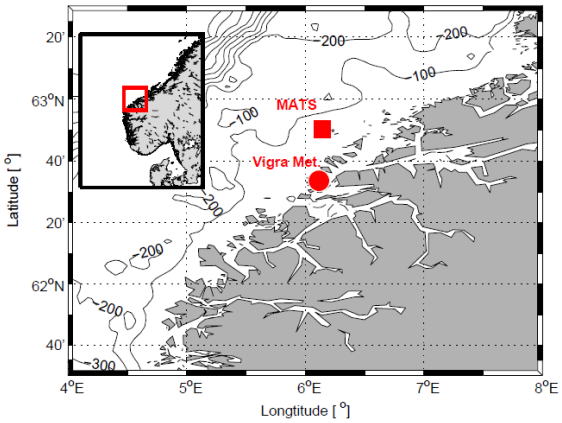

Fig. 2. Deployment site together with the isobaths at 100-m intervals. The position of MATS (filled rectangle) and the meteorological station Vigra (filled bullet) are marked. The inset shows the location in Norway.

Wave measurements from subsurface moving pressure sensor

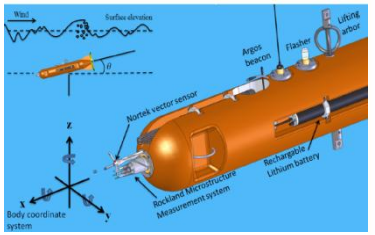

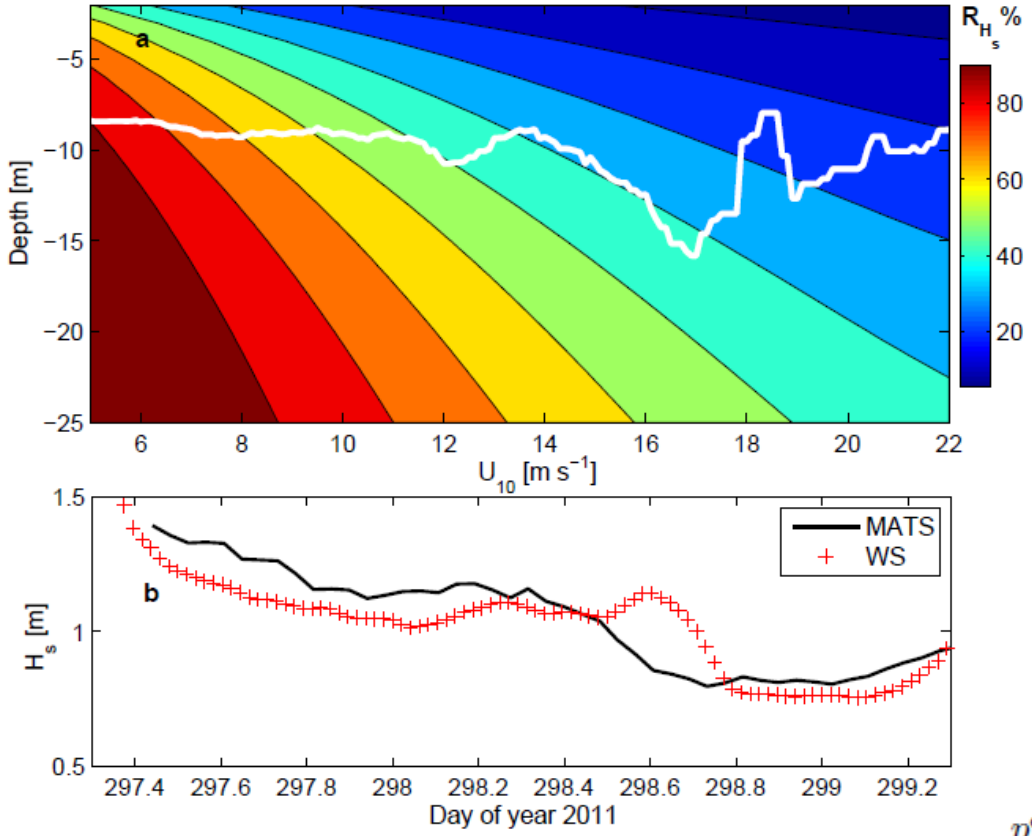

$$a_z = -g\cos\theta + \ddot{\zeta},$$

$$p_d^{obs} = \overbrace{\rho_w g K_p \eta(x,t)}^{p_d} - \overbrace{\int_{\tau'}\int_{t'} a_z(t')dt'd\tau'}^{\hat{\zeta}}.$$

Fig. 3. a) Pressure depth-attenuation relative error, $R_{Hs}(z,U_{10})$, in significant wave height, H_s, calculations based on the linear small-amplitude wave theory. R_{H_s} is a function of depth, z, and wind speed at a reference height of 10-m, b) Comparison between H_s measured by the Wave Scan (WS) in the vicinity of MATS (plus markers) and estimated from the MATS corrected pressure sensor data (solid line). The WS measurements are available for only 2 days.

From Bakhoday-Paskyabi & Fer 201 4 (NPG)

Wave measurements from subsurface moving pressure sensor

- Very good agreement with waverider buoy (BIOWAVE cruise 2011)

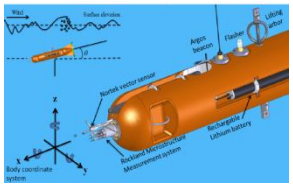

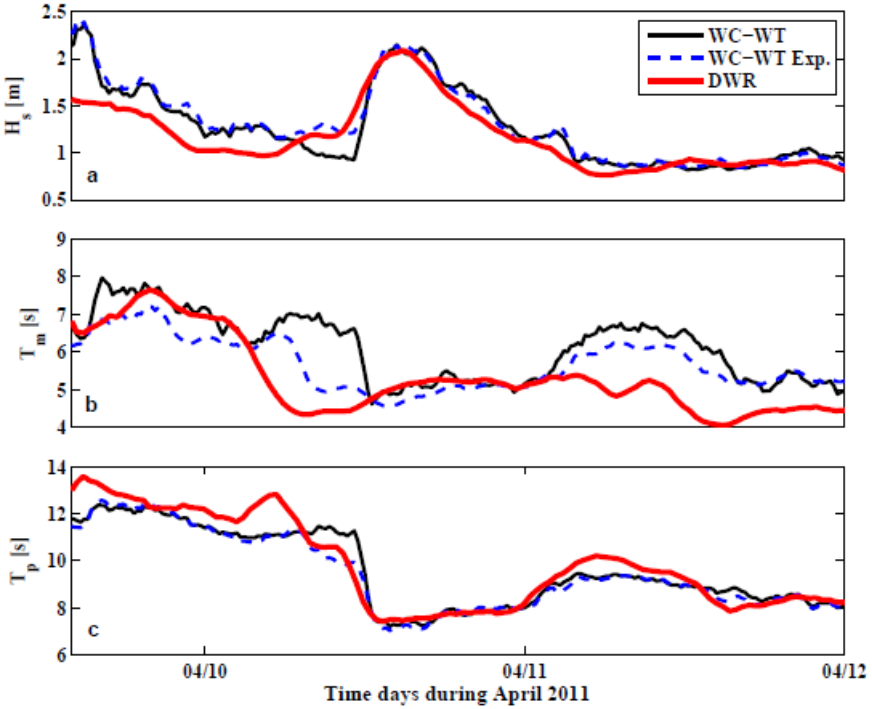

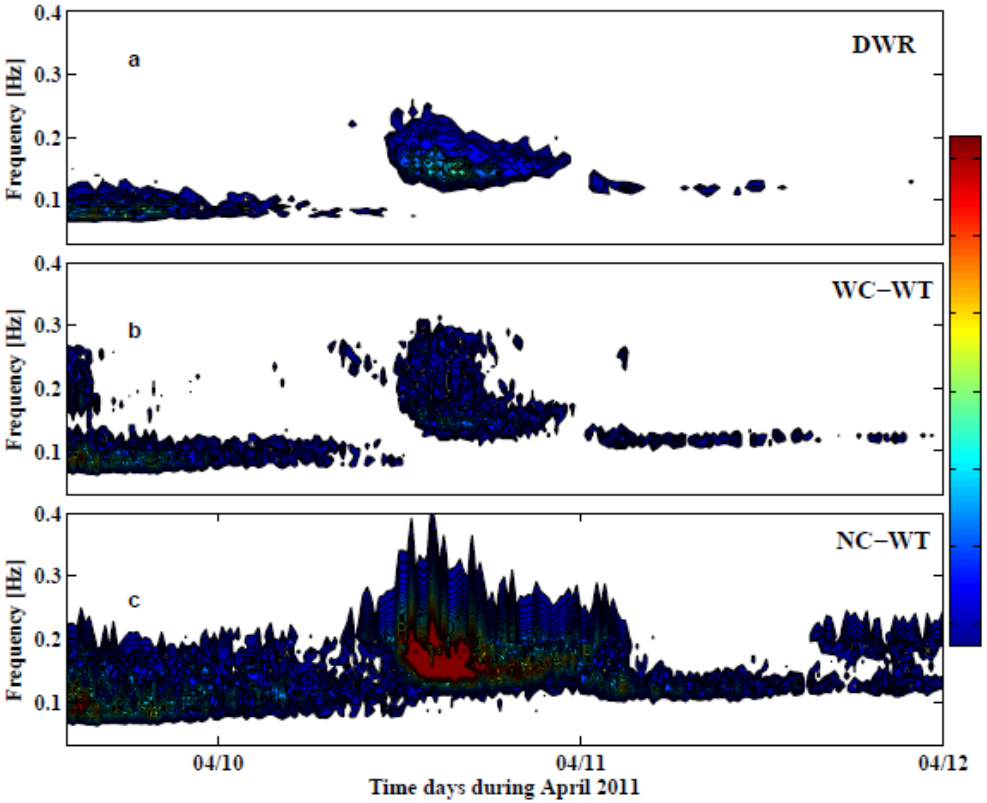

From Bakhoday-Paskyabi 2014 (submitting)

Wave and microstructure shear

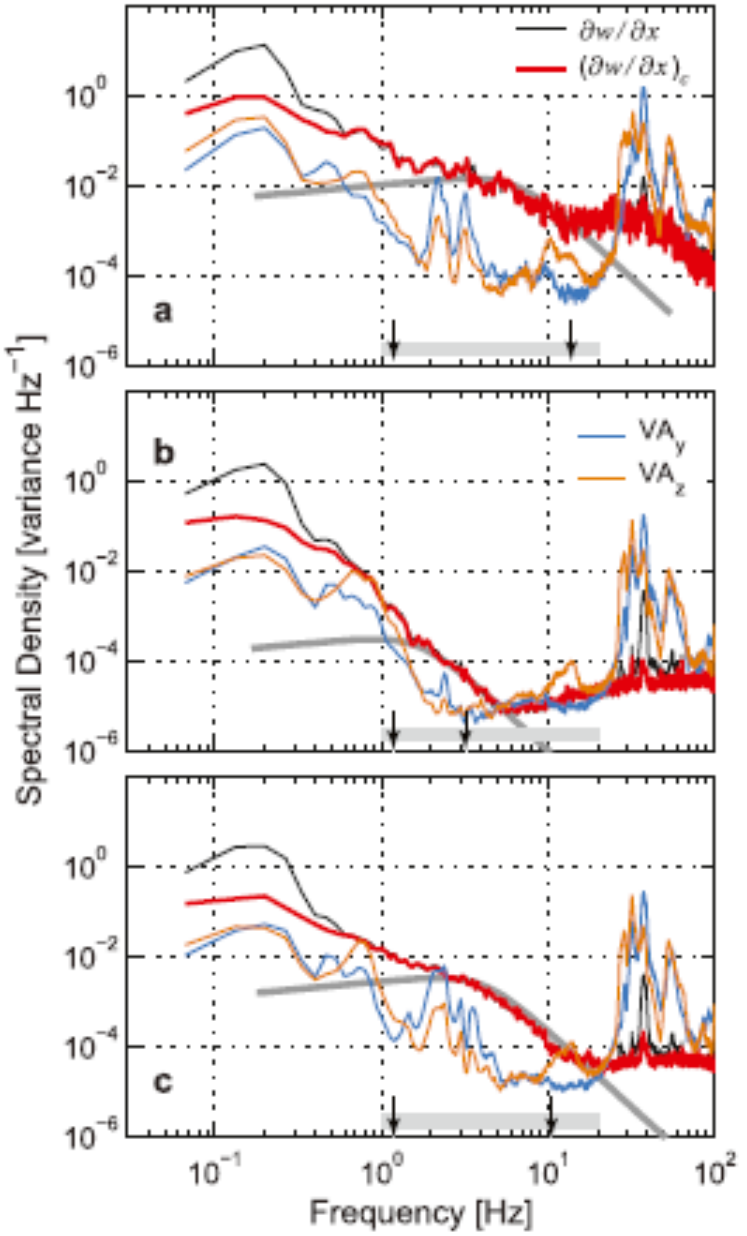

FIG. 10. As in Fig. 8, but for turbulence shear $\partial w/\partial x$ (black) and the two components of the piezo-accelerometers (vibration sensors), VA_y and VA_z. The thick red curves are the clean shear spectra after removing the parts of the signal coherent with the accelerometers $(\partial w/\partial x)_c$. Nasmyth's turbulence spectrum for the inferred average ε is shown by gray curves. The horizontal gray band shows the range of the spectra extracted for calculation of the dissipation rate. Note that this is not the integration band over which the shear variance is calculated, but it is the portion of the spectrum passed on to the routine that iteratively adjusts the integration band. Correction for the lost variance is a factor of 1.7 for periods 1 and 3 and 2 for period 2. Integration wavenumber band (arrows) is 4–50, 6–16, and 5–47 cpm. The number of 60-s segments that were averaged is 5, 10, and 25.

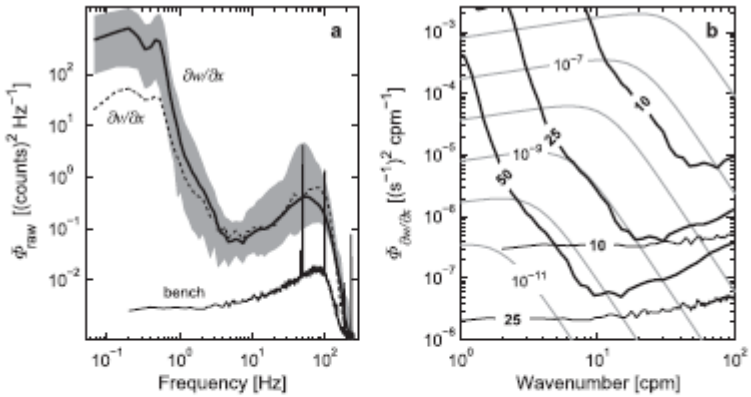

FIG. 11. Noise spectra for shear. (a) Frequency spectra of the raw output of the shear probes averaged for 199 segments, each lasting 60 s, when the shear variance was low. The thick black line is the spectrum from shear probe 1 ($\partial w/\partial x$) with gray-shaded region indicating the minimum and maximum ranges; the dashed line is the mean spectrum from shear probe 2 ($\partial u/\partial x$). Average spectra are band averaged in frequency in 60 logarithmically equally spaced bins. Spectrum from a 15-min-long record from a bench test in the laboratory using an open-circuit dummy probe is also shown as reference for the electronic noise. (b) Noise spectra inferred from quiescent shear spectra (thick curves) converted into physical units, and into wavenumber spectra, using a mean flow increasing from 10 to 50 cm s^{-1}. Gray curves are the spectral shapes after Nasmyth for ε of 10^{-6} to 10^{-11} W kg^{-1}. Corresponding electronic noise spectrum from the bench test (thin lines) is also shown for a mean flow of 10 and 25 cm s^{-1}.

TABLE 1. Overview of conditions during the selected three 15-min segments of the dataset. Here, H_s is the significant wave height; T_m and T_p are the mean and peak wave periods, respectively; W_{20m} is the wind speed at 20-m height; N_{15m} is the buoyancy frequency at 15-m depth; L_O is the Ozmidov length scale; u is the flow along the axis of the instrument; AOA is the angle of attack; and ε is the dissipation rate of TKE.

		1	2	3
Date	(2011)	10 Apr	12 Apr	12 Apr
Time	(UTC)	1440	0000	2000
H_s	(m)	2.0	1.0	0.9
T_m	(s)	5.3	4.7	7.1
T_p	(s)	7.7	7.9	13.0
W_{20m}	(m s^{-1})	13.5	0.7	11.0
N_{15m}	(s^{-1})	2.9×10^{-3}	5.3×10^{-3}	8.9×10^{-3}
L_O	(m)	7.8	0.2	0.6
u	(cm s^{-1})	17 ± 3	17 ± 2	18 ± 3
AOA	(°)	2.1 ± 0.4	2.3 ± 0.4	1.5 ± 0.3
ε	(W kg^{-1})	1.5×10^{-6}	8.4×10^{-9}	2.2×10^{-7}

Wave and microstructure shear

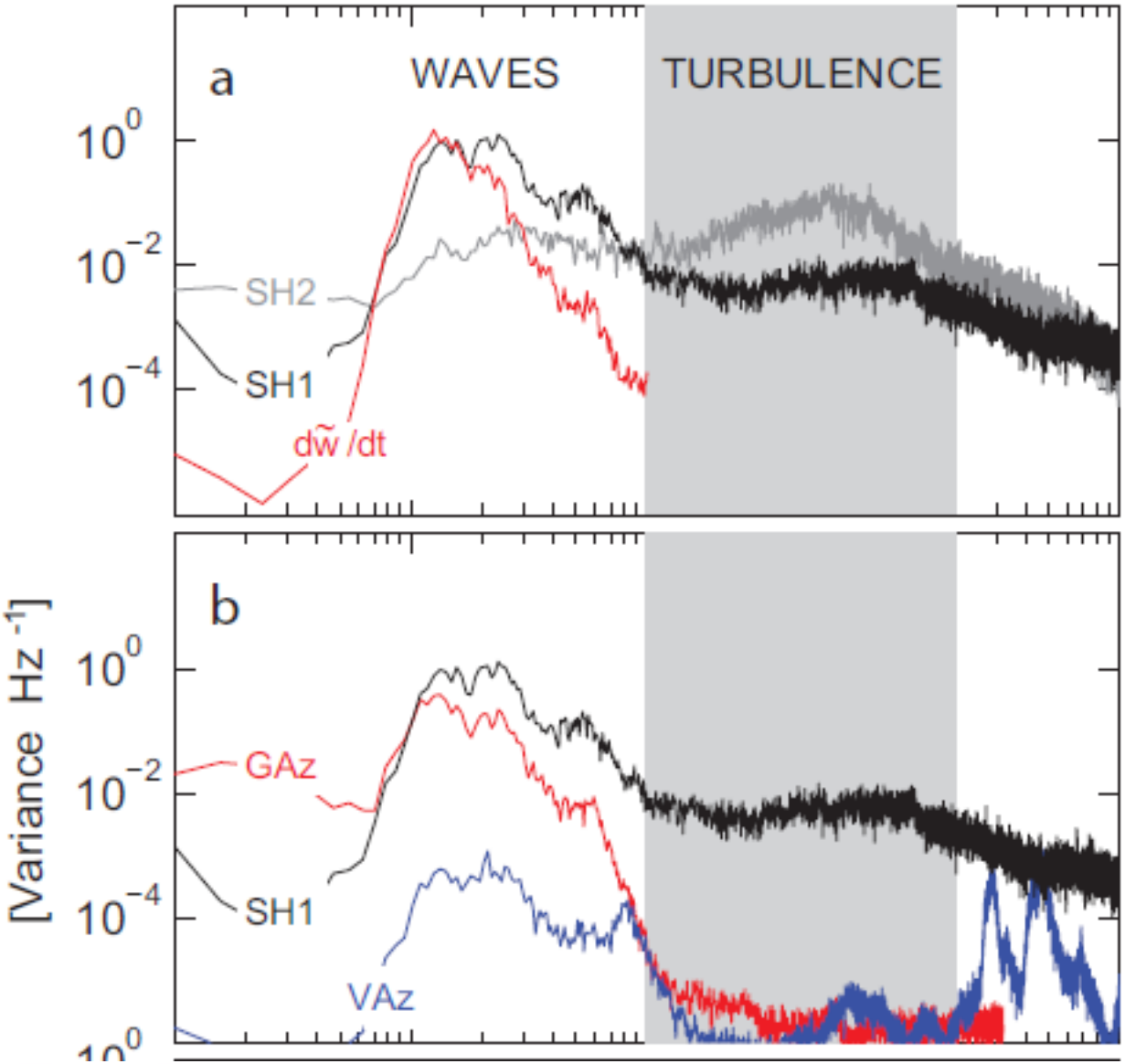

From Bakhoday-Paskyabi & Fer 2013 (JEP)

Wave and microstructure shear

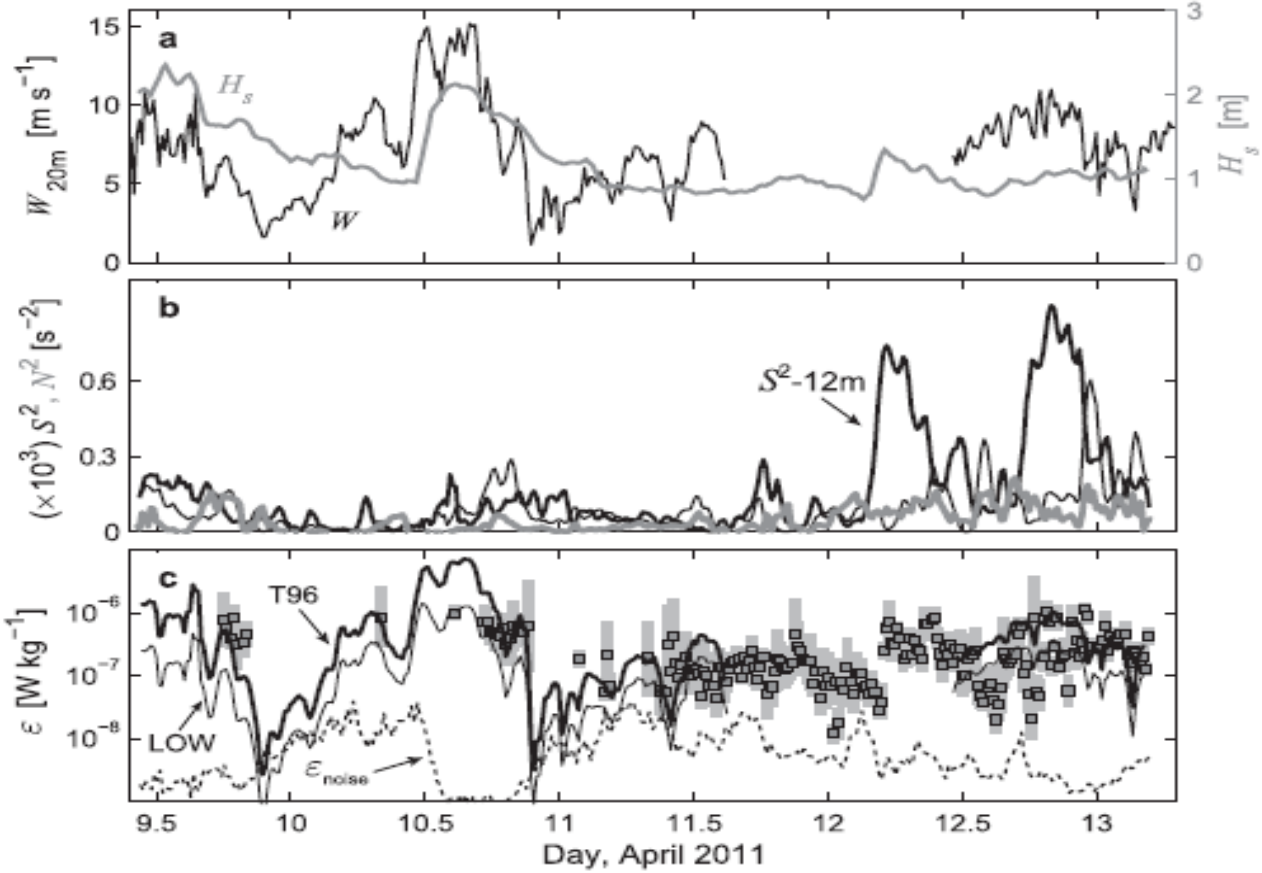

FIG. 13. Time series of measured dissipation rate of TKE, ε. Selected environmental forcing parameters are also shown for reference. (a) Wind speed W_{20m} and significant wave height H_s as in Fig. 7. (b) Shear-squared (black) and buoyancy frequency squared (gray), 4-m first difference inferred between bins at 10 and 14 m (S^2-12m), and 6-m first difference between 12 and 18 m, where joint velocity and density measurements are available (thin black, S^2-15m, and gray, N^2-15m). (c) Dissipation rate, 15-min averages, and 95% confidence intervals (markers and gray bars). Thick black line marked T96 is the ε predicted by the Terray et al. (1996) scaling [Eq. (8)]. Thin line indicates the dissipation expected from LOW. Wind speed measurements and friction velocity (hence wind speed) dependent T96 and LOW during the period when the ship was moored near land are excluded. The dashed curve is the lowest detection level of dissipation rate ε_{noise} estimated as a function of the mean flow.

From Fer & Bakhoday-Paskyabi 2014 (JTEC)

Numerical Modelling

Governing equations

$$\frac{\partial u}{\partial t} = -\frac{\partial(\overline{u'w'})}{\partial z} + f_{cor}(v + v_s) + F_x,$$
$$\frac{\partial v}{\partial t} = -\frac{\partial(\overline{v'w'})}{\partial z} - f_{cor}(u + u_s) + F_y,$$
$$\frac{\partial T}{\partial t} = -\frac{\partial(\overline{T'w'})}{\partial z} - \frac{\partial R}{\partial z},$$
$$\frac{\partial S}{\partial t} = -\frac{\partial(\overline{S'w'})}{\partial z},$$

$$\rho_w K_m \frac{\partial u}{\partial z} = \boldsymbol{\tau}_a - \boldsymbol{\tau}_{in} - \boldsymbol{\tau}_{ds},$$
$$K_h \frac{\partial T}{\partial z} = \frac{Q_T}{\rho_w C_p},$$
$$K_h \frac{\partial T}{\partial z} = \frac{(E_v - P_r)S_0}{\rho_w},$$

$$\frac{\partial \bar{e}}{\partial t} = \overbrace{-\left(\overline{u'w'}\frac{\partial U}{\partial z} + \overline{v'w'}\frac{\partial V}{\partial z}\right)}^{P_{curr}} - g\frac{\overline{\rho'w'}}{\rho_w} \overbrace{-\frac{\partial}{\partial z}(\overline{e'w'}) - \frac{1}{\rho_w}\frac{\partial}{\partial z}(\overline{p'w'})}^{1} - \varepsilon,$$

$$P_{mech} = P_{curr} + P_{Stokes} + P_{wb}. \quad P_{Stokes} = -\overline{u'w'}\frac{\partial u_s}{\partial z} - \overline{v'w'}\frac{\partial v_s}{\partial z} \quad P_{wb}(z) = -\frac{1}{\rho_w}\frac{\partial \overline{p'w'}(z)}{\partial z},$$

Parameterizations

(LOW): $$\varepsilon = \frac{u_{*w}^3}{\kappa|z|},$$

$$\varepsilon(z) = \begin{cases} \frac{0.3F_k}{H_s}(0.4)^{-2}, & 0 < z < 0.6H_s; \\ \frac{0.3F_k}{H_s}\left(\frac{z}{H_s}\right)^{-2}, & 0.6H_s \le z < z_t; \\ \frac{u_{*w}^3}{\kappa(D-z)}, & -D < z < z_t. \end{cases}$$

$$\varepsilon = u_{*w}^2\left(\frac{dU}{dz} + \frac{dU_s}{dz}\right)\exp\left[2\sqrt{\frac{dU}{dz}\frac{dU_s}{dz}}T_L\right],$$

$$\frac{\varepsilon_B(z=h/2)}{u_{*a}^3/h} = A_s + A_L La^{-2} + A_c La^{-2}\frac{h}{L_L},$$

where ε_B denotes the parametrization of the dissipation rate at $z = h/2$ as suggested by Belcher et al. (2012), $A_s = 2(1-\exp(-La/2))$, $A_L = 0.22$, and $A_c = 0.3$. Figure 1.3 shows contours of $\log_{10}\varepsilon/\varepsilon_B$ in La–h/L_L regime diagram.

Parameterizations

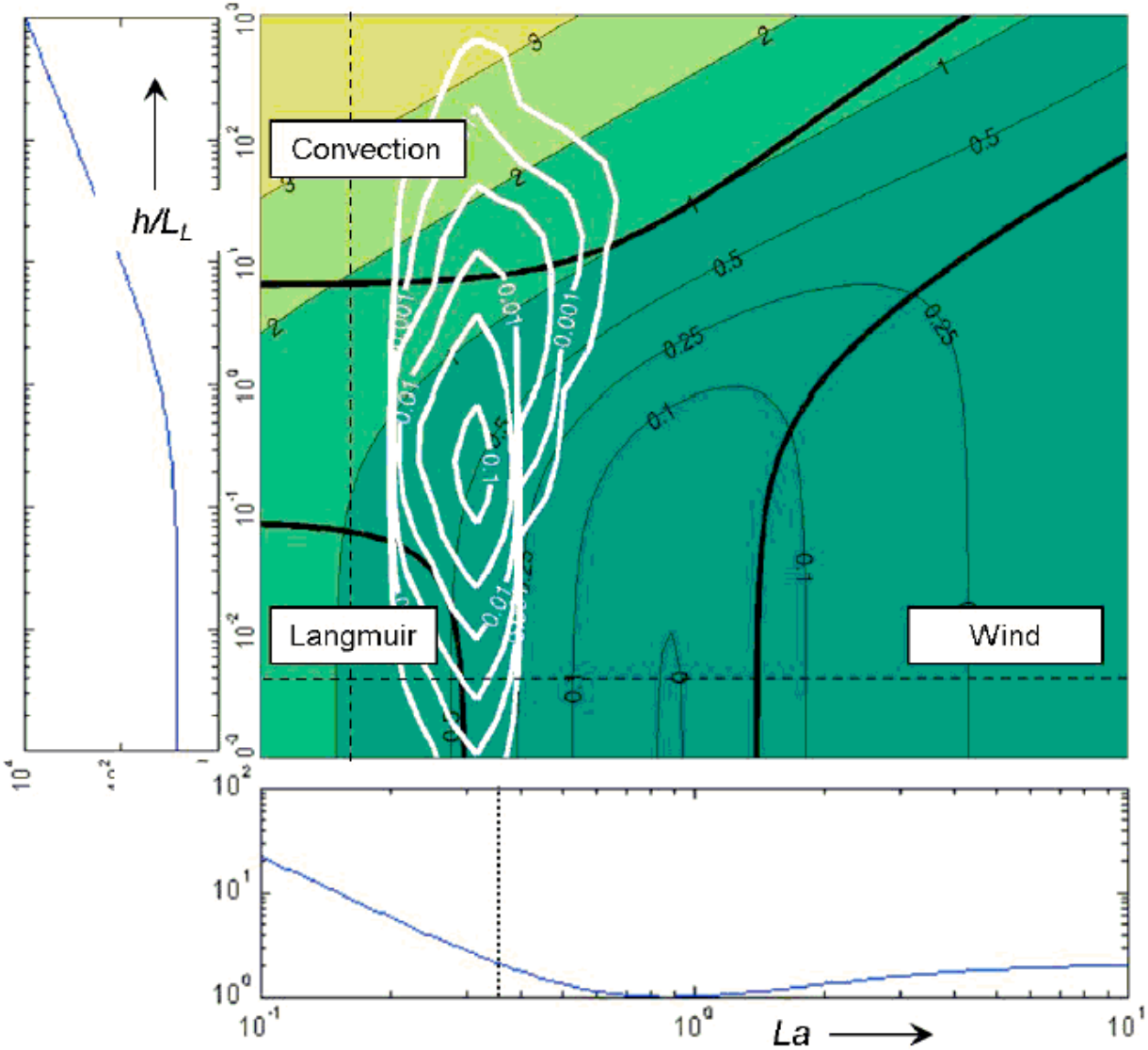

From Belcher et. al 2012

Air-sea interaction

- Modification on 1D general ocean turbulence model by including wave effects
- Enhancement of mixing near surface
- More realistic representation of mixed layer deepening

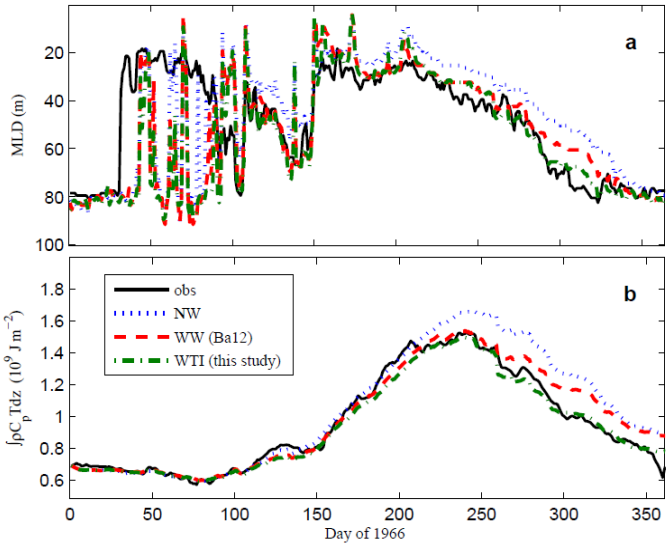

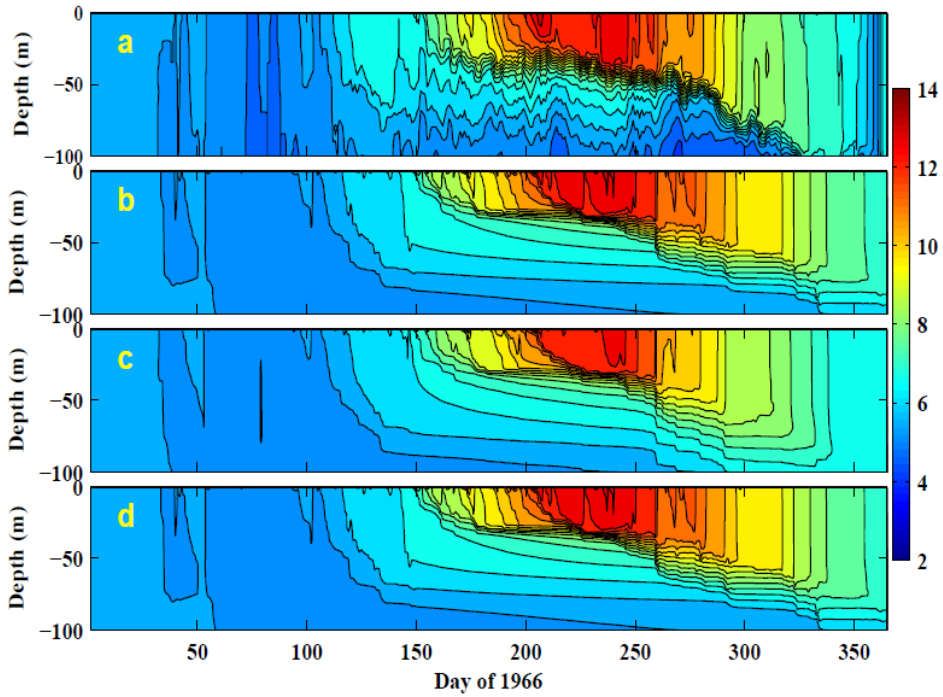

Fig. 2. *Top*: Temperature evolution at OWS Papa in the northern Pacific Ocean for year 1966, (a) observations, (b) GOTM run with wave forcing effects based on [13], (c) GOTM with the wave–turbulence interaction modification, (d) GOTM without wave–forcing. *Bottom*: Temporal variability of (a) MLD and (b) heat content in the upper 50 m.

Bakhoday Paskyabi, M., I. Fer, and A. D. Jenkins (2012). Surface gravity wave effects on the upper ocean boundary layer: modification of a one-dimensional vertical mixing model. *Continental Shelf Research*, *38* (*63-78)*,

Jenkins, AD Bakhoday Paskyabi, M; Fer, I; Gupta, A K; Adakudlu, Mr (2012): Modelling the effect of ocean waves on the atmospheric and ocean boundary layers, *Energy Procedia.*

From Bakhoday-Paskyabi & Fer 2013

Comparisons with measurements

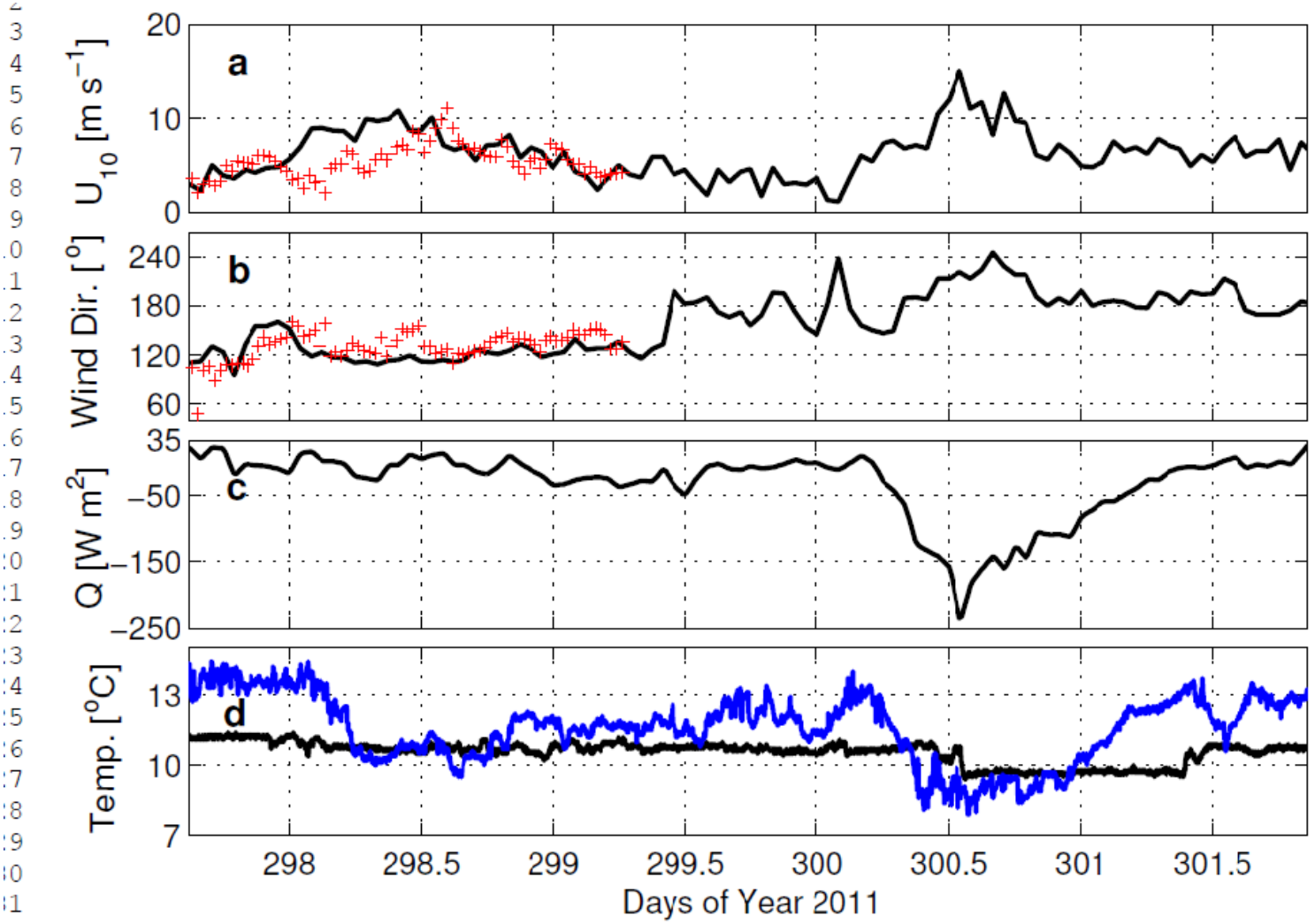

Fig. 2 Time series of (a) wind speed at 10 m height, U_{10}, from Vigra station (solid line), and from WS buoy (plus makers), (b) wind direction at 10 m height from Vigra station (solid line), and from WS buoy (plus markers), (c) total surface heat flux, and (d) water and air temperature at air–sea interface (black and blue solid lines, respectively) for the duration of the experiment on October 25 to 30 2011.

From Bakhoday-Paskyabi & Fer 2013

Comparisons with measurements

Fig. 4 Evolution of **a** the wave energy spectra calculated from the MATS's corrected pressure sensor in units of $m^2\ Hz^{-1}$, and **b** the Stokes drift in $m\ s^{-1}$. Both parameters are shown in the logarithmic scale

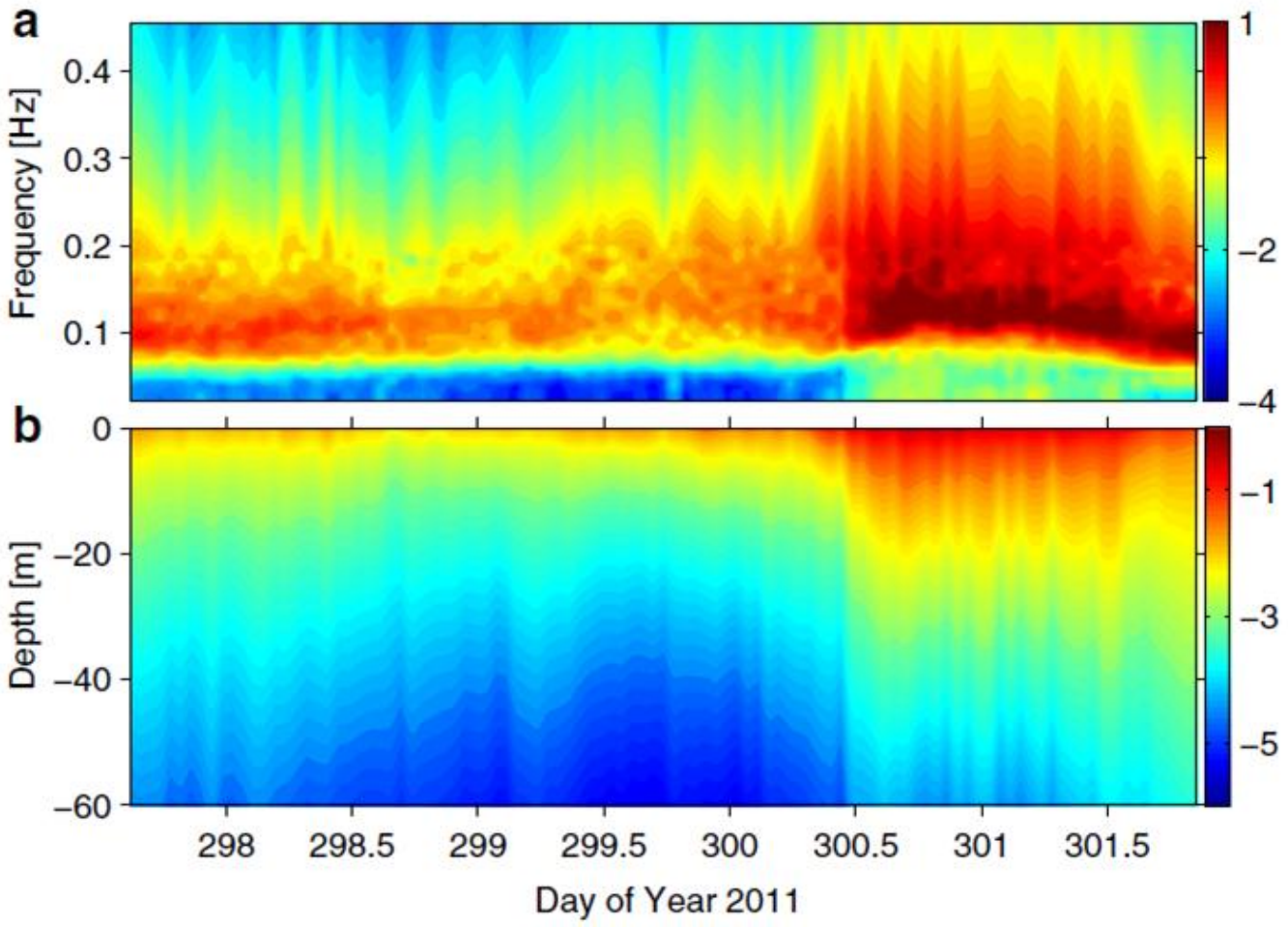

From Bakhoday-Paskyabi & Fer 2013

Comparisons with measurements

Fig. 5 Time series of **a** the wind stress components τ_w^x and τ_w^y, measured at the Vigra station, **b** the surface Stokes drift speed, **c** inverse of wave age, and **d** the Langmuir turbulence number, La_t.

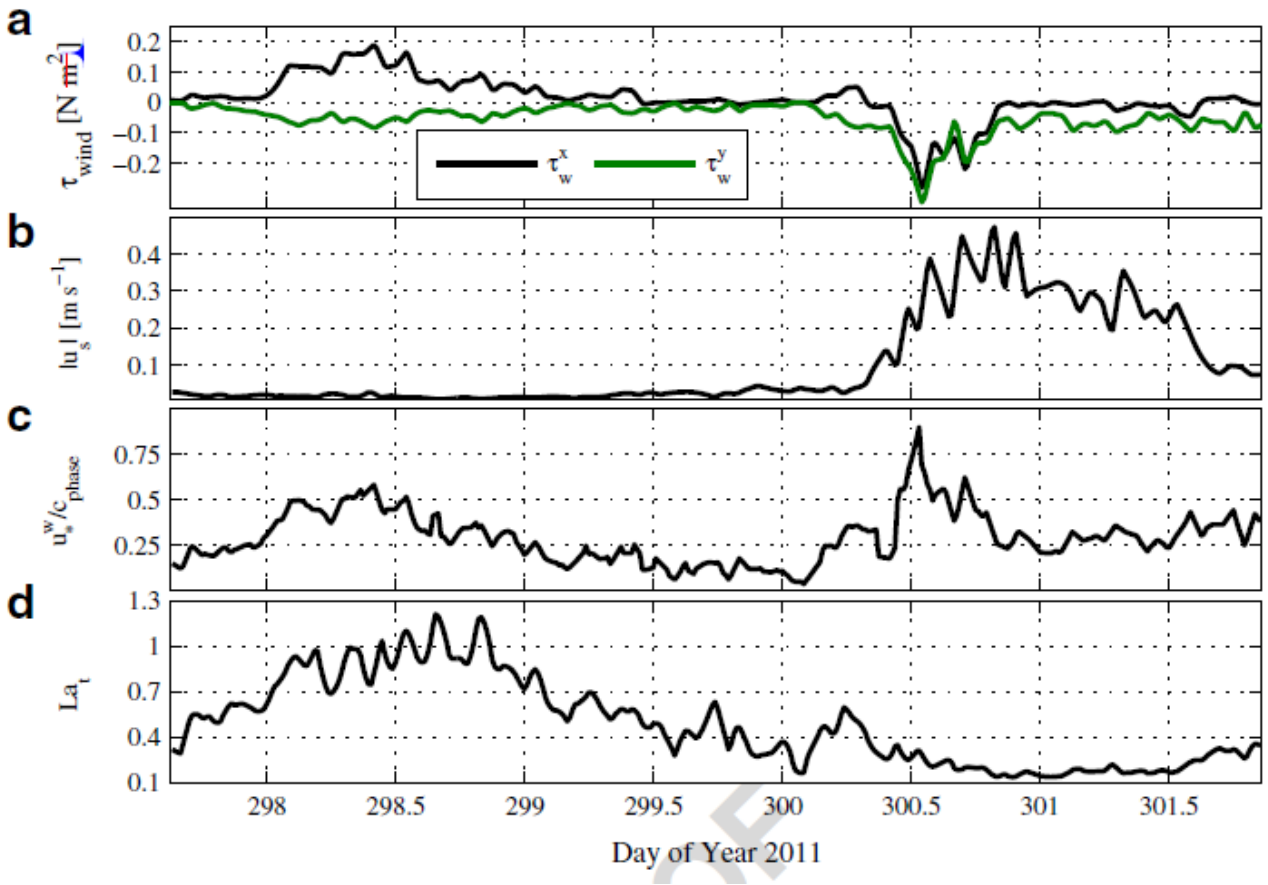

From Bakhoday-Paskyabi & Fer 2013

Comparisons with measurements

Table 1 MSS profiling periods during the experiment in October 2011

	Start	End	Duration	Casts
Set 1	25 14:56	25 21:49	6.9	51
Set 2	27 06:05	27 21:49	15.7	133
Set 3	28 06:04	28 08:04	2	18
Set 4	29 17:03	29 23:53	6.8	54

Start and end times are given as day in October and time in UTC. The duration is in hours

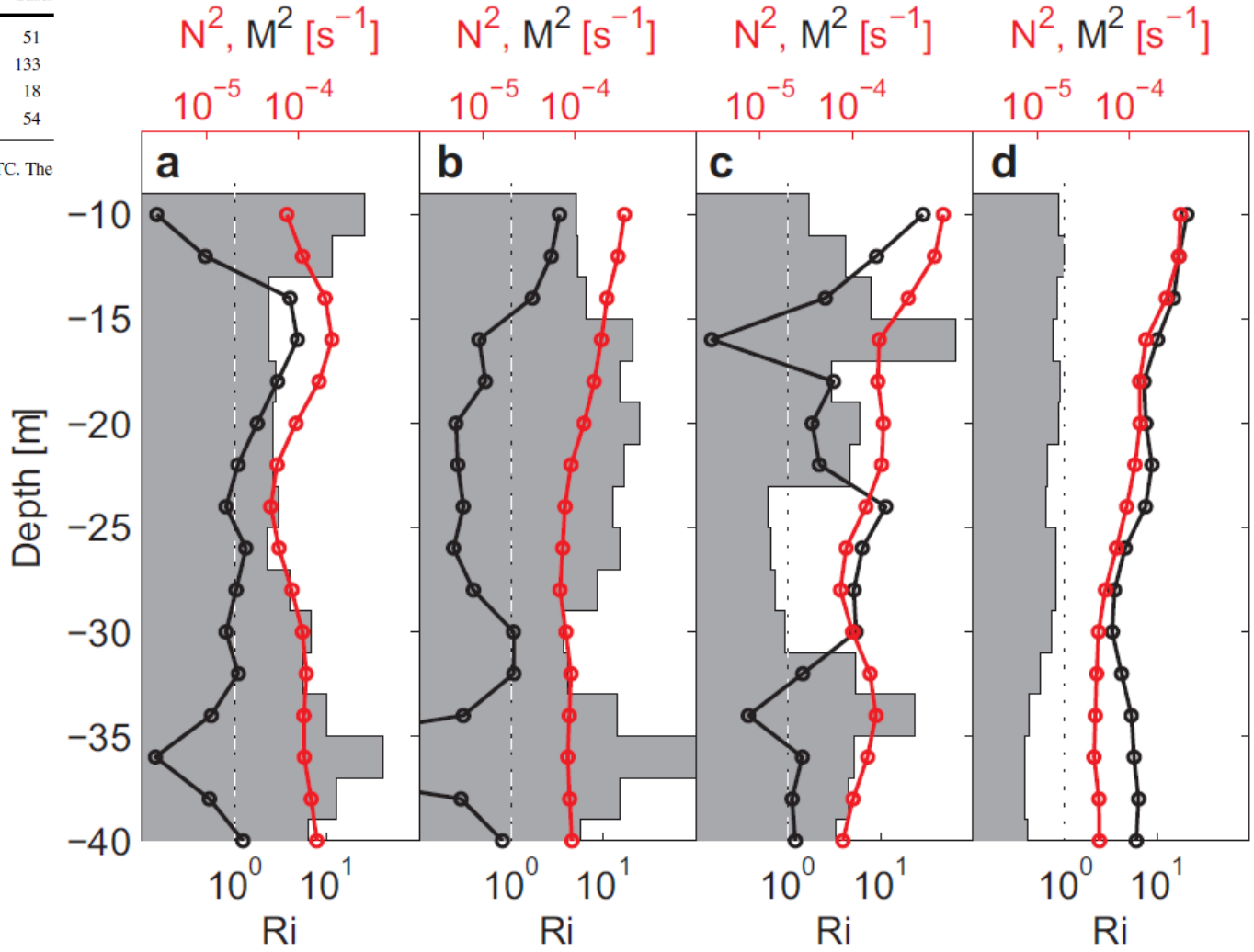

Fig. 11 Time averaged vertical profiles of squared shear M^2 (black solid lines), squared buoyancy N^2 (red solid lines), and $Ri = N^2/M^2$ (gray): (a) periods between 297.5 and 297.8, (b) between 299.4 and 299.9, (c) between 300.35 and 300.4, and (d) between 301.8 and 302.

Comparisons with measurements

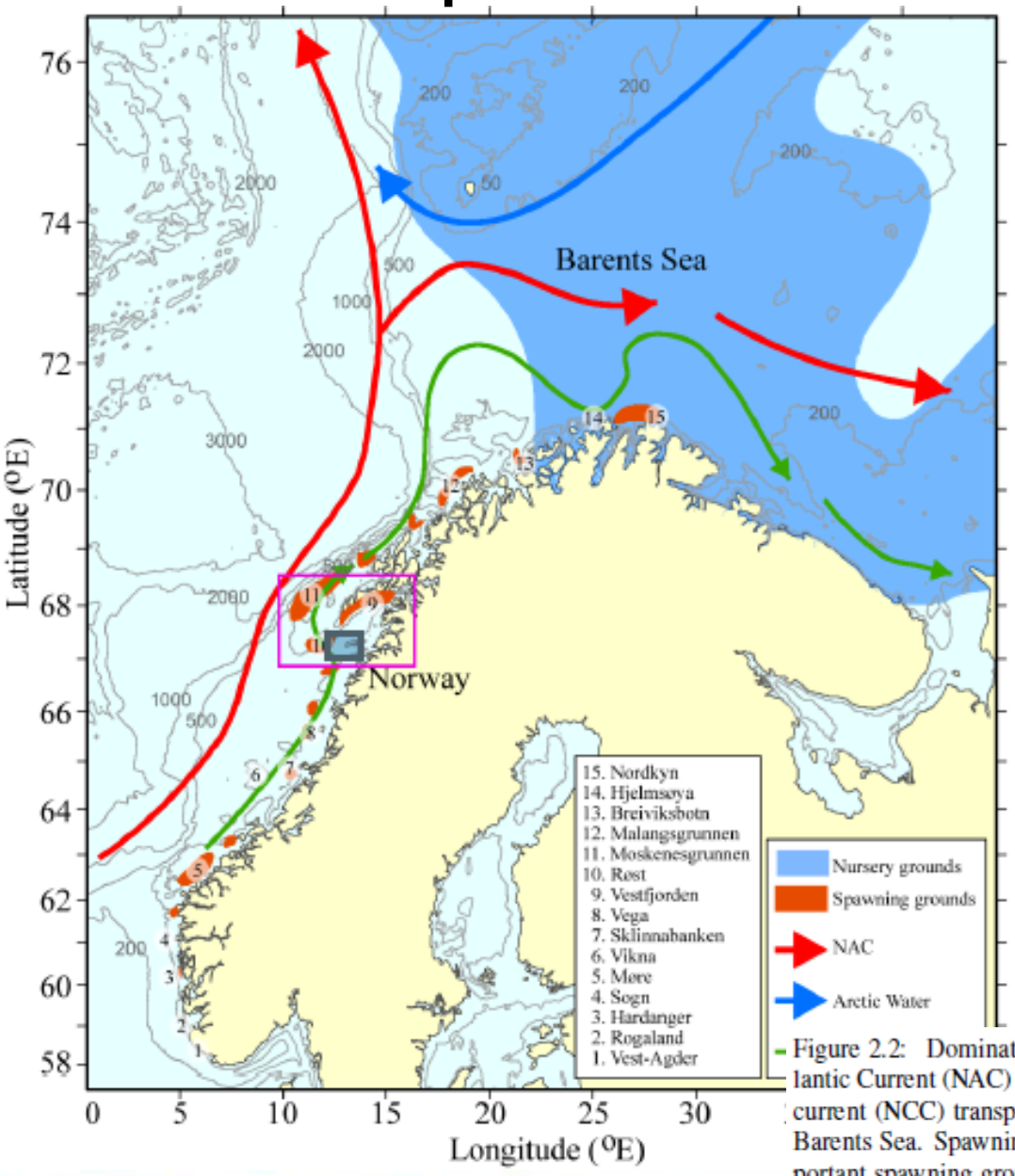

Figure 2.2: Dominating currents in the Norwegian Sea and the Barents Sea. The North Atlantic Current (NAC) transports warm and saline water northwards and the Norwegian coastal current (NCC) transports cold and fresh water from river runoff along the coast towards the Barents Sea. Spawning grounds of the NEA cod are marked as orange patches, the most important spawning ground is in the Vestfjorden bay (patch number 9). The nursery ground of the juveniles is the Barents Sea. A detailed map of the circulation in Vestfjorden, outlined by a pink box, is shown in Fig. 2.4. From Myksvoll et al. (2013).

From Bakhoday-Paskyabi & Fer 2013

Comparisons with measurements

Table 3 Numerical run details

Name	SP Eq. 37	SP Eq. 17	CSF Eq. 4	WB Eqs. 25 and 29
NW	No	No	No	No
W1	No	Yes	Yes	Yes
W2	Yes	No	Yes	Yes

The run without wave forcing is NW. Two simulation runs with wave forcing (W1 and W2 runs, respectively) include Stokes Production (SP), CSF, and Wave Breaking (WB) effects as listed

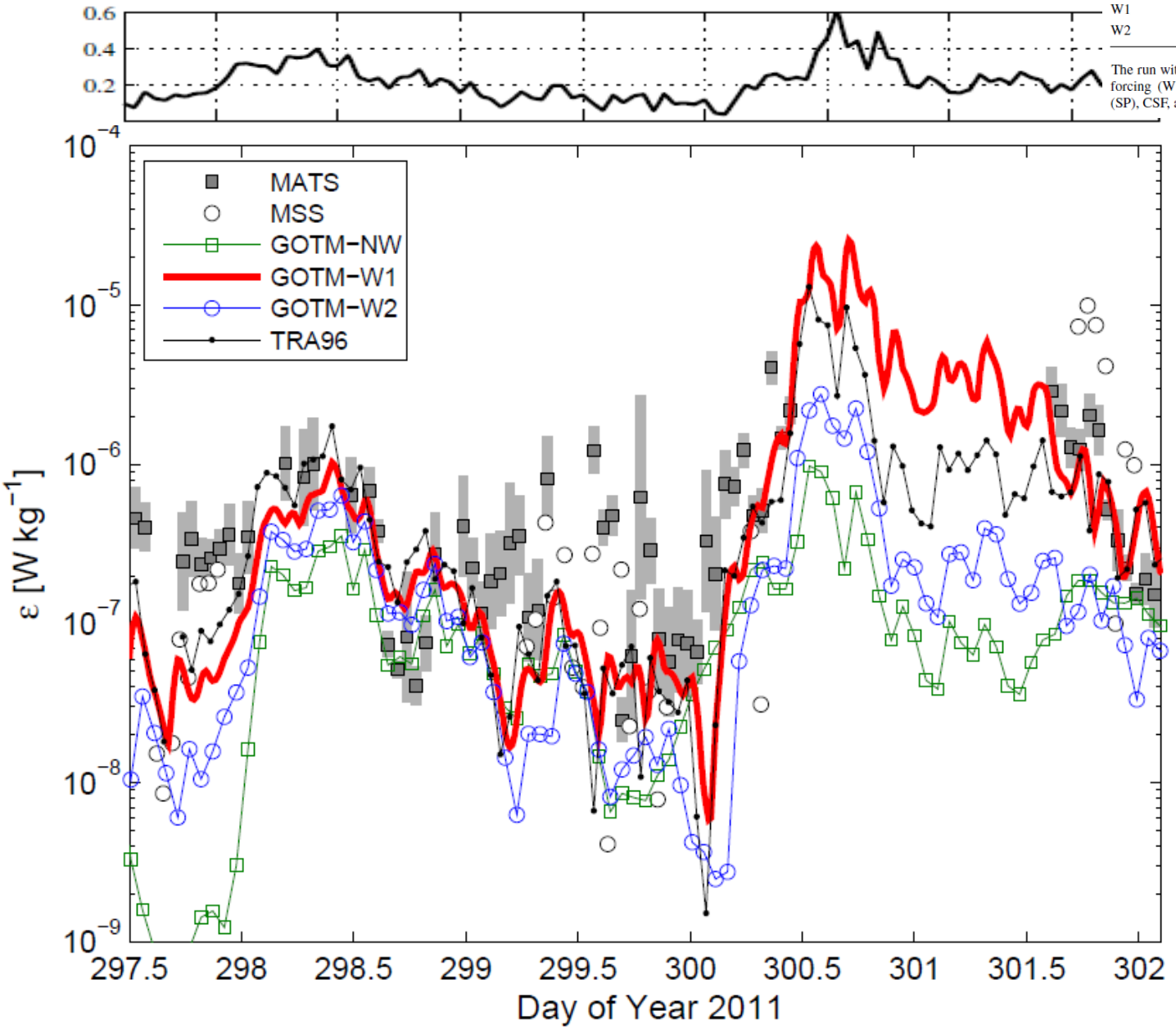

From Bakhoday-Paskyabi & Fer 2013

Comparisons with measurements

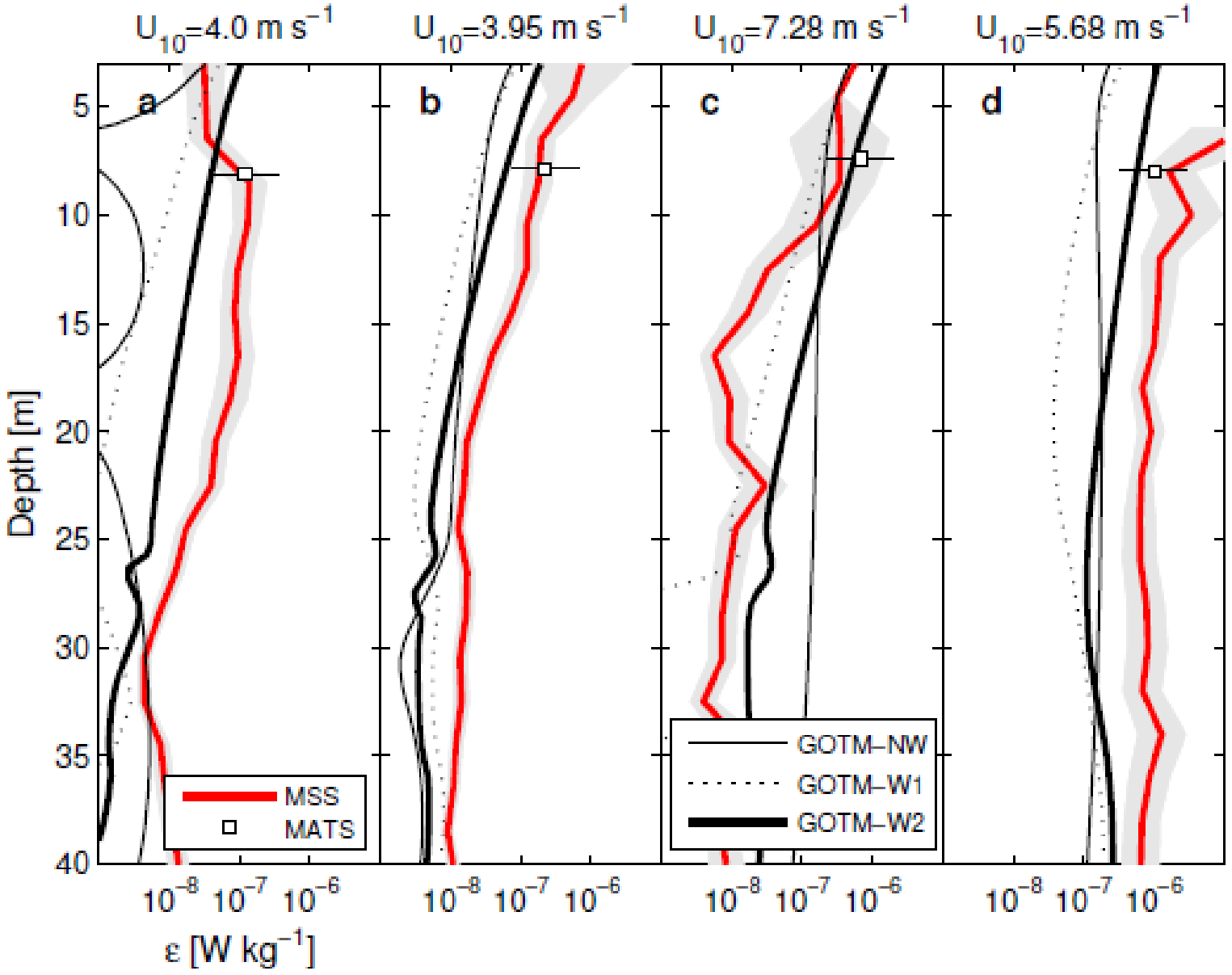

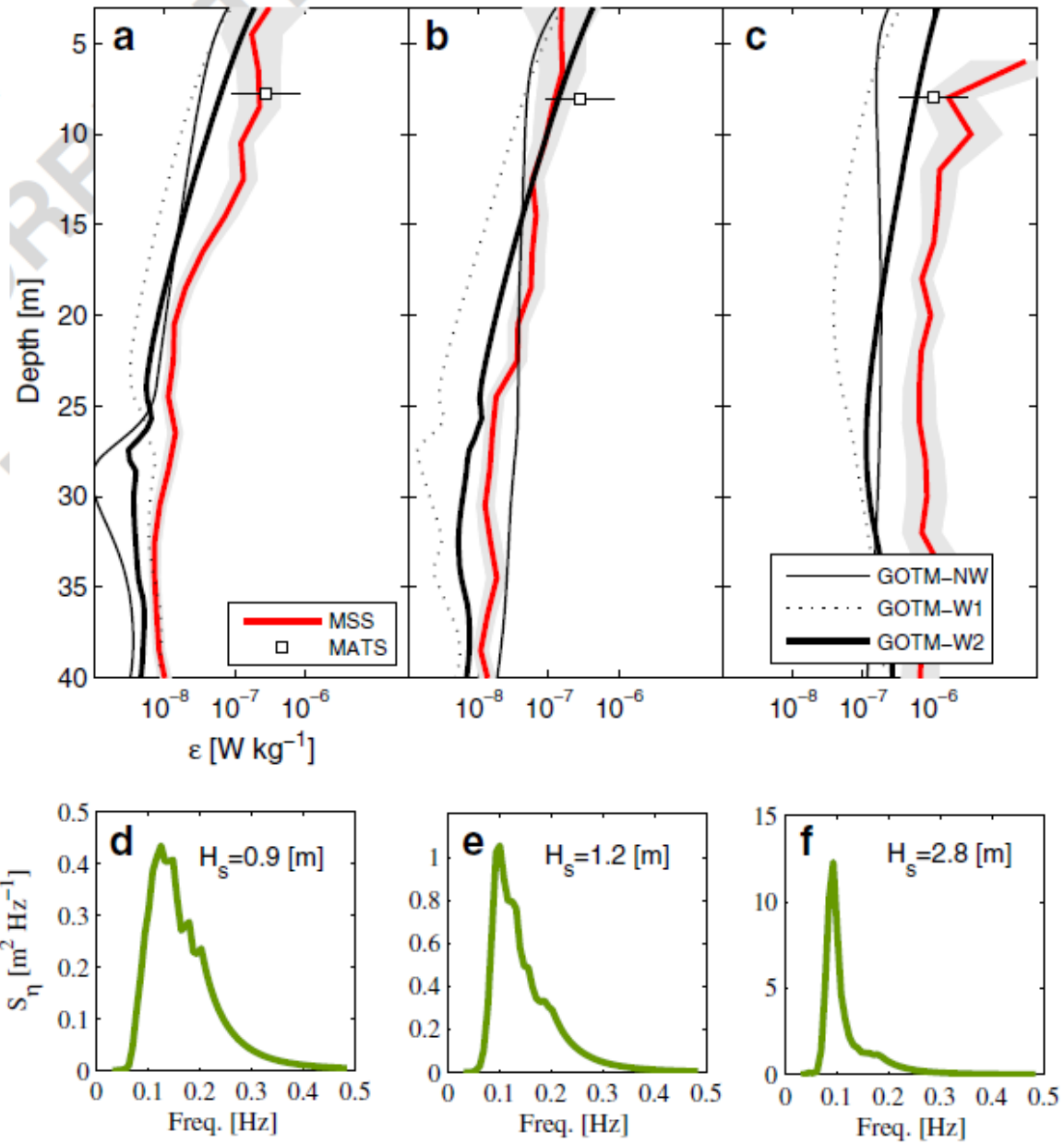

Fig. 14 Dissipation rates of TKE profiles in logarithmic scale for the three different wave conditions. Confidence intervals for MSS measurements of ε are denoted by the *shaded gray* regions. Shown are the results from the simulations NW (*solid lines*), W1 (*dotted lines*), and W2 (*thick solid lines*), the observed data from MSS profiler (*red solid lines*), and MATS at a fixed level (*square markers*) for **a** calm sea state, **b** moderate waves, and **c** high waves. *Lower panels* show the wave energy spectrum, S_η, estimated using pressure sensor mounted on MATS for **d** calm sea state, **e** moderate waves, and **f** high waves

Conclusions

[1] **M. Bakhoday Paskyabi** and I. Fer (2013), Turbulence structure in the upper ocean: a comparative study of observations and modeling, *Ocean Dynamic,* DOI: **10.1007/s10236-014-0697-6**.

[2] **Bakhoday Paskyabi, M**., I. Fer, and A. D. Jenkins (2012), Surface gravity wave effects on the upper ocean boundary layer: modification of a one-dimensional vertical mixing model. *Continental Shelf Research*, *Volume 38*, *Pages 63-78*.

[3] Jenkins, Alastair David; **Bakhoday Paskyabi, Mostafa**; Fer, Ilker; Gupta, Alok Kumar; Adakudlu, Muralidhar (2012): Modelling the effect of ocean waves on the atmospheric and ocean boundary layers*, Journal of Energy Procedia.*

[4] **Bakhoday Paskyabi, M**., I. Fer, and A. D. Jenkins (2012), Upper Ocean Response to Large Wind Farm Effect in the Presence of Surface Gravity Waves. *Journal of Energy Procedia.*

[5] I. Fer, **M. Bakhoday-Paskyabi** (2013), Autonomous ocean turbulence measurements with a moored instrument, accepted in *JTECH*.

[6] **M. Bakhoday Paskyabi**, Martin Flugge, J.E Edson, and J. Rueder (2013), Wave-induced characteristics of atmospheric turbulence flux measurement, *Energy Procedia*.

[7] **M. Bakhoday Paskyabi**, I. Fer (2013), The influence of surface gravity waves on the injection of turbulence in the upper ocean, under review in *Nonlinear Processes in Geography*.

[8] **M. Bakhoday Paskyabi** (2013), Perturbation in the acoustic field from a large offshore wind farm in the presence of surface gravity waves, *Energy Procedia*.

[9] Martin Flugge, **M. Bakhoday Paskyabi**, J.E. Edson, and J. Rueder (2013), Comparison of Direct Covariance Flux 1 Measurements from a 2 tower and a discus buoy, submitted in *JTECH*.

[10] **M. Bakhoday Paskyabi** and I. Fer (2013), Turbulence Measurements from Moving Platform in Shallow Water, *Energy Procedia*.